

Chemisorption and dissociation of single oxygen molecules on Ag(110)

J. R. Hahn^{a)} and W. Ho*Department of Physics and Astronomy and Department of Chemistry, University of California, Irvine, California 92697-4575*

(Received 18 March 2005; accepted 6 October 2005; published online 6 December 2005)

The chemisorption of single oxygen molecules on Ag(110) and the dissociation of the adsorbed molecules induced by tunneling electrons were studied at 13 K using a variable-low-temperature scanning tunneling microscope. Two predominant types of chemisorbed O₂ molecules were identified, one with the O₂ molecular axis aligned along the [001] direction of the substrate [O₂(001)], and the other with the molecular axis aligned along the [1 $\bar{1}$ 0] direction [O₂(1 $\bar{1}$ 0)]. Tunneling of electrons between the scanning tunneling microscope tip and O₂(001) caused the molecule either to rotate or dissociate, depending on the direction of electron tunneling. In contrast, electron tunneling caused O₂(1 $\bar{1}$ 0) to dissociate regardless of tunneling direction. In addition to O₂(001) and O₂(1 $\bar{1}$ 0), several other oxygen species and their dynamical behaviors were observed. © 2005 American Institute of Physics. [DOI: [10.1063/1.2131064](https://doi.org/10.1063/1.2131064)]

I. INTRODUCTION

The well-known activity of silver as a catalyst for selective oxidation of hydrocarbons^{1,2} has generated a number of investigations devoted to the molecular level understanding for the interaction of oxygen with silver surface.^{3–5} Since the interaction of oxygen with silver surface involves several adsorbed states, it has served as a model system for the study of adsorption and dissociation. The adsorption of oxygen on a Ag(110) surface has been characterized by three distinct states:^{6,7} a molecular physisorbed state, a molecular chemisorbed state, and a dissociative (atomic) chemisorbed state. In the physisorbed state (below 40 K), O₂ molecules lie on the surface with the molecular axis aligned along the [001] direction.⁸ The chemisorbed state (40–150 K) has been widely studied using various techniques,^{8–17} however, conflicting results have been reported regarding the characteristics of the chemisorbed molecule including its charge state. O₂ molecules adsorbed at temperatures above 150 K undergo dissociation.¹⁸ At room temperature or above, such dissociative adsorption induces changes in the surface structure such as the formation of adrows along the [001] direction.^{19,20} Although several studies have examined this dissociation process,^{19–25} the development of a model for the dissociation has been hindered by the existence of conflicting evidence about the orientation of the chemisorbed O₂, and by the narrow temperature range between the dissociation of the chemisorbed O₂ and the surface reconstruction.

In this paper, we report atomic-scale images of oxygen species chemisorbed on Ag(110) at 45–75 K and of the rotation and dissociation process of the O₂ molecules initiated by tunneling electrons, which were obtained using a variable-low-temperature scanning tunneling microscope (STM). The

STM images reveal two types of chemisorbed O₂, two types of O atoms, and an O₂–O complex species. The rotation and dissociation pathways of each type of adsorbed O₂ molecules depend on the tunneling direction of the electrons.

II. EXPERIMENT

Experiments were carried out using a homebuilt variable-low-temperature STM,²⁶ housed inside an ultrahigh-vacuum chamber with a base pressure of 2×10^{-11} Torr. The Ag(110) sample was cleaned by repeated cycles of 500 eV Ne ion sputtering and 693 K annealing. The STM tip was made by electrochemical etching of polycrystalline tungsten wire and further cleaned *in situ* by Ne ion self-sputtering and annealing. The STM tip was then reshaped by field emission and light physical contacts with the surface. During exposure of the Ag(110) surface to O₂ molecules, the temperature was maintained between 40 and 75 K to ensure molecular chemisorption. An O₂ coverage of less than 0.01 ML (monolayer) was employed to permit investigation of individual well-isolated molecules. After adsorption was complete, the sample and the STM were cooled to 13 K to minimize thermal drift in the tip-sample junction. At 13 K, a very small number of CO molecules (<0.001 ML) were additionally adsorbed onto the surface; the transfer of one of these CO molecules to the apex of the STM tip enabled atomically resolved imaging.^{27–29} The tunneling bias voltage in the STM junction was applied to the sample.

III. RESULTS

A. Two types of chemisorbed O₂ molecules

Inspection of numerous STM topographical images of O₂ molecules chemisorbed on a Ag(110) surface revealed two predominant types of chemisorbed O₂; representative STM images of these two types are shown in Fig. 1. One type of O₂ appears as an oval-shaped depression with a

^{a)} Author to whom correspondence should be addressed: Department of Chemistry, Chonbuk National University, Jeonju 561-756, Korea. Electronic mail: jrhahn@chonbuk.ac.kr

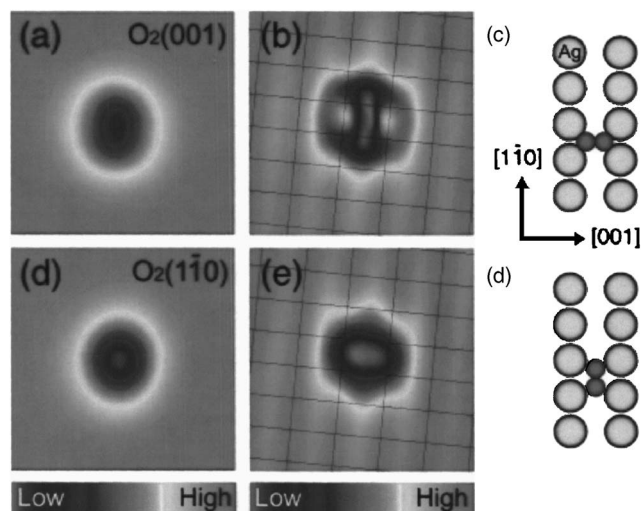


FIG. 1. O_2 molecules chemisorbed on Ag(110). The left column shows topographical images obtained using a bare tip at a voltage of 70 mV and a tunneling current of 1 nA [(a) and (d)]. The center column shows atomically resolved topographical images obtained using a CO-terminated tip at a voltage of 70 mV and a tunneling current of 1 nA [(b) and (e)]. The grid lines are drawn through the Ag surface atoms. The schematic diagrams of the adsorption sites are shown in the right column [(c) and (f)]. The small circles represent O atoms and the large circles represent Ag atoms. The sizes of the circles are scaled to the atomic covalent radii. [(a)–(c)] An O_2 molecule chemisorbed on the fourfold hollow site with its molecular axis aligned along the $[001]$ direction [$O_2(001)$]. [(d)–(f)] An O_2 molecule chemisorbed on the fourfold hollow site with its molecular axis aligned along the $[1\bar{1}0]$ direction [$O_2(1\bar{1}0)$]. The scan area of images (a), (b), (d), and (e) is $25 \times 25 \text{ \AA}^2$.

maximum depth of 0.4 \AA when imaged using a bare metallic tip [Fig. 1(a)], and as a depression with two prominent protrusions when imaged using a CO-terminated tip [Fig. 1(b)]. The other type of O_2 also shows an oval-shaped depression when imaged with a bare tip [Fig. 1(d)], although the depth of this depression is slightly greater than that of the other type of O_2 . When this second type was imaged using a CO-terminated tip, the shape of the image was modified but no protrusions appeared [Fig. 1(e)]. The images of the two types of O_2 obtained using a bare tip [Figs. 1(a) and 1(d)] are difficult to tell apart because the only distinguishing feature is a very slight difference in depth. In contrast, the STM images obtained using the CO-terminated tip [Figs. 1(b) and 1(e)] are easily distinguished. The atomically resolved images of the Ag(110) surface obtained using a CO-terminated tip revealed that the two types of adsorbed O_2 lie in the same type of fourfold hollow but have different orientations, as shown schematically in Figs. 1(c) and 1(f). The molecular axis of the adsorbed O_2 shown in Figs. 1(a) and 1(b) is aligned along the $[001]$ direction [$O_2(001)$], whereas the molecular axis of the other type of O_2 [Figs. 1(d) and 1(e)] is aligned along the $[1\bar{1}0]$ direction [$O_2(1\bar{1}0)$]. Such alignment is concluded based on the dissociation pathways (see below), and the spatial symmetry of the electronic orbital and vibrational intensity of the $O_2(001)$.²⁹ It was determined that a dissociation pathway of the $O_2(001)$ involved the conversion to the $O_2(1\bar{1}0)$ and then the two O atoms were always found to lie along the $[1\bar{1}0]$ direction (see below).

TABLE I. Relative population of oxygen species produced by O_2 exposure on Ag(110) at 45 and 75 K. See the text for the notification.

Dosing temperature	$O_2(001)$	$O_2(1\bar{1}0)$	O_2-O_{sb}	O_{fth}
45 K	0.39	0.55	0.06	<0.01
75 K	0.40	0.54	0.06	<0.01

Table I lists the statistical populations of $O_2(001)$, $O_2(1\bar{1}0)$, and other oxygen species (described below), as determined from inspection of approximately 1000 images of individual adsorbed oxygen molecules. No significant difference in the distribution was observed between 45 and 75 K. The most abundant species is $O_2(1\bar{1}0)$. The ratio $O_2(001)/O_2(1\bar{1}0)$ is 0.71.

B. Rotation and dissociation of O_2 by positive bias voltage pulses

The tunneling of electrons from the STM can induce an $O_2(001)$ to rotate 90° to form an $O_2(1\bar{1}0)$. This was achieved by positioning the STM tip over an $O_2(001)$ molecule and then applying a positive voltage pulse between 450 and 470 mV of 25 s duration at a tunneling current of 1 nA to the sample with the feedback off. The threshold voltage for the rotation was found to be 450 mV. This rotation is irreversible and occurs only with a positive voltage pulse.

Tunneling of electrons from the STM tip to $O_2(1\bar{1}0)$, on the other hand, causes the oxygen molecule to dissociate rather than to rotate. Specifically, application of a positive voltage pulse of 480 mV to the sample with the STM tip positioned over the center of an $O_2(1\bar{1}0)$ molecule caused the molecule to dissociate into two O atoms lying along the $[1\bar{1}0]$ direction. STM imaging revealed dissociated O atoms at three different separations: nearest-neighbor [Figs. 2(a)–2(c)], next-nearest neighbor [Figs. 2(d)–2(f)], and next-next-nearest neighbor [Figs. 2(g)–2(i)]. The depression of the nearest-neighbor O atoms [Fig. 2(a)] is the deepest. It should be mentioned that a prolonged positive voltage pulse on the $O_2(001)$ also led to the dissociation into two oxygen atoms whose separations were similar to those observed after the dissociation of $O_2(1\bar{1}0)$.

Because the voltage pulse was applied with the feedback off, the tunneling current varied when the molecule or atom under the tip changed during the application of the pulse. Such a variation of the tunneling current was recorded during the application of a voltage pulse of 480 mV to an $O_2(001)$ molecule, as shown in Figs. 2(j) and 2(k). Here, the times at which the oxygen state changed are indicated by a sudden decrease of tunneling current in Fig. 2(j) and a sudden decrease followed by an increase in Fig. 2(k). The variation of the tunneling current should be related to the depth in the STM image. For example, the change from $O_2(001)$ to the dissociated nearest-neighbor O atoms causes the depth of the image to become deeper, and hence causes the sudden decrease of tunneling current shown in Fig. 2(j). The variation of tunneling current induced by the rotation of $O_2(001)$ to $O_2(1\bar{1}0)$ is too small to be observed because of the small

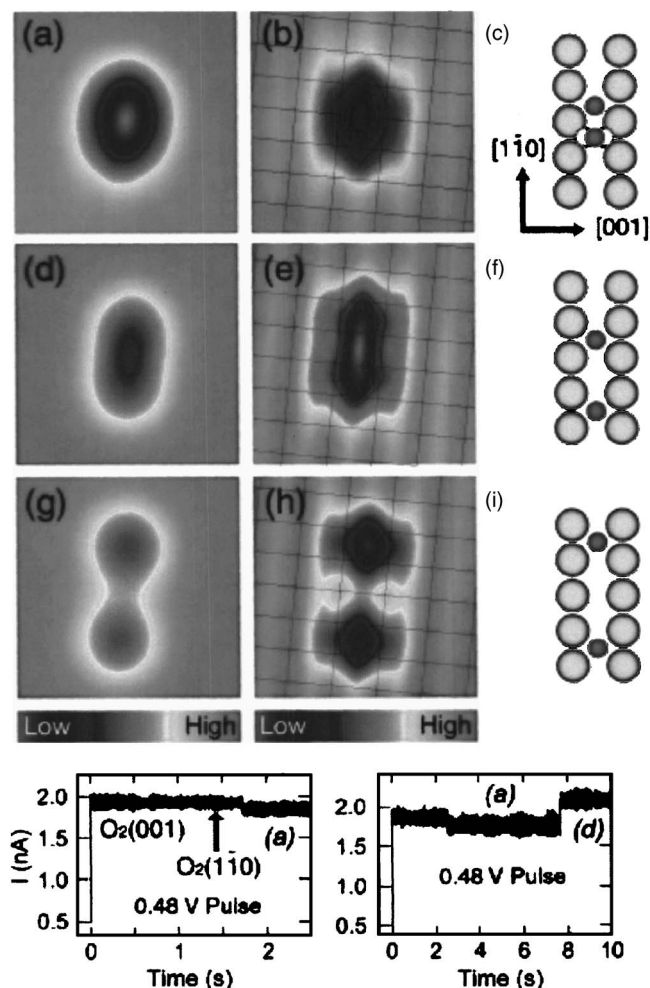


FIG. 2. Dissociation of an $O_2(001)$ molecule chemisorbed on Ag(110) by a positive voltage pulse at 13 K. The left column shows topographical images obtained using a bare tip at a voltage of 70 mV and a tunneling current of 1 nA [(a), (d), and (g)]. The center column shows atomically resolved topographical images obtained using a CO-terminated tip at a voltage of 70 mV and a tunneling current of 1 nA [(b), (e), and (h)]. Schematic diagrams of the adsorption sites are shown in the right column [(c), (f), and (i)]. A positive voltage pulse (+480 mV) on $O_2(001)$ [Fig. 1(a)] with the feedback off led to the formation of either [(a)–(c)] nearest-neighbor oxygen atoms, or [(d)–(f)] next-nearest-neighbor oxygen atoms, or [(g)–(i)] next-next-nearest-neighbor oxygen atoms. The dashed circles in (c) indicate the geometry of the original $O_2(001)$ molecule prior to dissociation. (j) The variation of tunneling current during applying the voltage pulse, which led to the formation of the nearest-neighbor atoms (a). (k) The variation of tunneling current during application of the voltage pulse, which led to the formation of the nearest-neighbor atoms (d).

difference in the depths of their STM images. Either stopping the voltage pulse upon detecting a sudden change in the tunneling current or controlling the pulse period makes it possible to selectively control the product.

C. Dissociation of O_2 by negative bias voltage pulses

The $O_2(001)$ molecule is also dissociated by negative voltage pulses, although different products are formed. Figure 3 shows the details of the dissociation pathway induced by a voltage pulse of -370 mV on $O_2(001)$. The pathway involves the formation of an O–O complex [Figs. 3(a) and 3(b)] followed by the separation of this complex along the [001] direction into two separate O atoms [Figs. 3(d) and

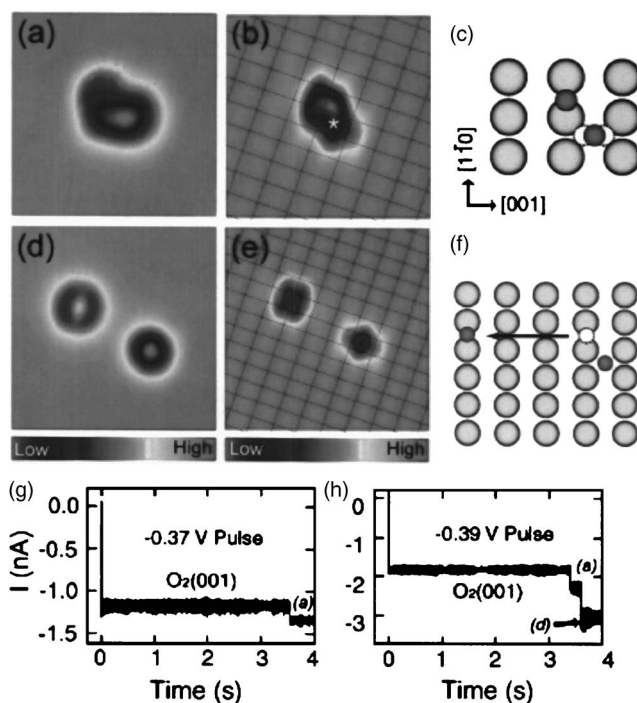


FIG. 3. Dissociation of an $O_2(001)$ molecule chemisorbed on Ag(110) by a negative voltage pulse at 13 K. The negative voltage pulse (-370 or -390 mV) on $O_2(001)$ [Fig. 1(a)] with the feedback off led to the formation of [(a)–(c)] an O–O complex or [(d)–(f)] two atoms separated along the [001] direction. The dashed circles in (c) indicate the geometry of the original $O_2(001)$ molecule prior to dissociation. (j) The variation of tunneling current during application of the voltage pulse, which led to the formation of the O–O complex (a). (k) The variation of tunneling current during application of the voltage pulse, which led to the formation of the two atoms shown in (d). The scan area of images (a) and (b) is $27 \times 27 \text{ \AA}^2$ and the scan area of images (d) and (e) is $37 \times 37 \text{ \AA}^2$. All images were obtained at a sample bias of 70 mV and a tunneling current of 1 nA.

3(e)], one adsorbed at the fourfold hollow site (O_{fh}) and the other bonded to the short-bridge site (O_{sb}). The O–O complex is an intermediate of the dissociation process that appears as an $O_{\text{fh}}-O_{\text{sb}}$ structure in the atomically resolved image obtained using a CO-terminated tip [Fig. 3(b)]. Imaging the same area before and after the dissociation allowed us to probe the trajectory of the O atoms during dissociation. The O_{fh} atom remains on the position of the original $O_2(001)$ while the O_{sb} moves away along the [001] direction a distance of more than 10 \AA . The threshold voltage for dissociation was determined to be -390 mV (± 10 mV) under application of a negative voltage pulse (with a pulse duration of 25 s at a tunneling current of 1 nA). The formation of the $O_{\text{fh}}-O_{\text{sb}}$ complex and subsequent full separation were accompanied by sudden decreases in the tunneling current [Figs. 3(g) and 3(h)].

The atomic positions in the $O_{\text{fh}}-O_{\text{sb}}$ complex shown in Figs. 3(a) and 3(b) can be switched by tunneling electrons. A voltage pulse of -270 mV on complex I [* in Fig. 4(a)] with the feedback off caused it to convert to complex-II [Fig. 4(b)]. The tunneling current during the pulse [Fig. 4(c)] switches between two distinct current levels, where the lower and higher currents correspond to complexes I and II, respectively. The complex is fixed on the Ag atom between the two

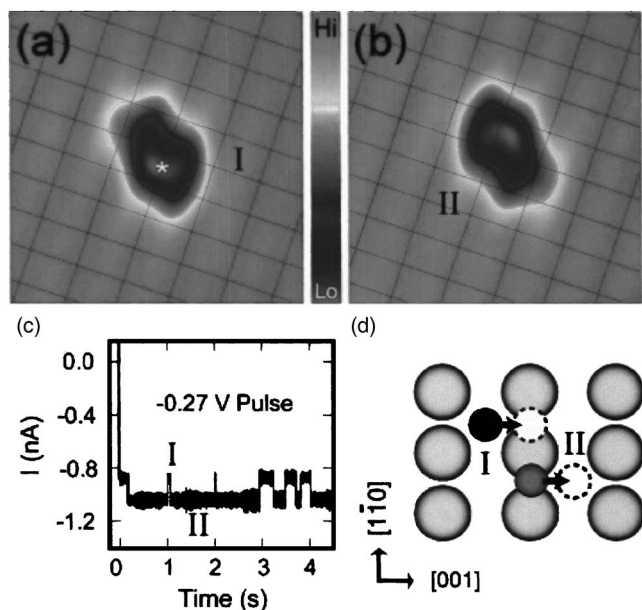


FIG. 4. Switching of the adsorption geometry of the O–O complex [Fig. 3(b)] by a negative voltage pulse (-270 mV). The voltage pulse on the position (*) in (a) led to a switching of the positions of the O atoms at the fourfold hollow and short-bridge sites. (a) and (b) STM images of the O–O complexes obtained using a CO-terminated tip at a sample bias of 70 mV and a tunneling current of 1 nA. (c) The variation of tunneling current during application of the voltage pulse. “I” and “II” in the images indicate the geometries of (a) and (b), respectively. (d) Schematic diagram of the adsorption geometry for the complex. The arrows indicate the trajectory of the two atoms.

O atoms, and does not diffuse on the surface. Both atoms in the complex simultaneously move to form an equivalent complex about the same Ag atom, as illustrated in Fig. 4(d). This observation indicates that the two atoms interact with each other through the Ag atom.

D. O₂–O complexes

In addition to the individual O₂ molecules and O atoms, we also observed a complex comprised of an O₂ molecule and an O atom as a result of O₂ adsorption at 45 K (Fig. 5). Four types of equivalent orientation were observed for the complex [Figs. 5(a)–5(d)]; the thermal energy at 13 K caused interconversion between these orientations within several minutes. Tunneling of electrons led to the dissociation of the complex into three O atoms, two O_{sb}, and one O_{fh} [Fig. 5(e)]. The atomic-scale image of the complex taken using a CO-terminated tip [Fig. 5(f)] shows a combination of an O₂ on the fourfold hollow site and an O_{sb}. The complexes may be produced when a highly mobile O_{sb} formed by thermal dissociation migrates across the surface and attaches to an O₂. There are four possible next-nearest short-bridge sites around the O₂ site, which leads to four types of orientations as shown in Fig. 5. The relative proportion of this species was about 6% (Table I). Even if the surface is dosed at temperatures low enough that only molecular chemisorption should occur (45–75 K), a very small number of molecules are likely to dissociate, as established previously using high-resolution electron-energy-loss spectroscopy (HREELS).¹⁶

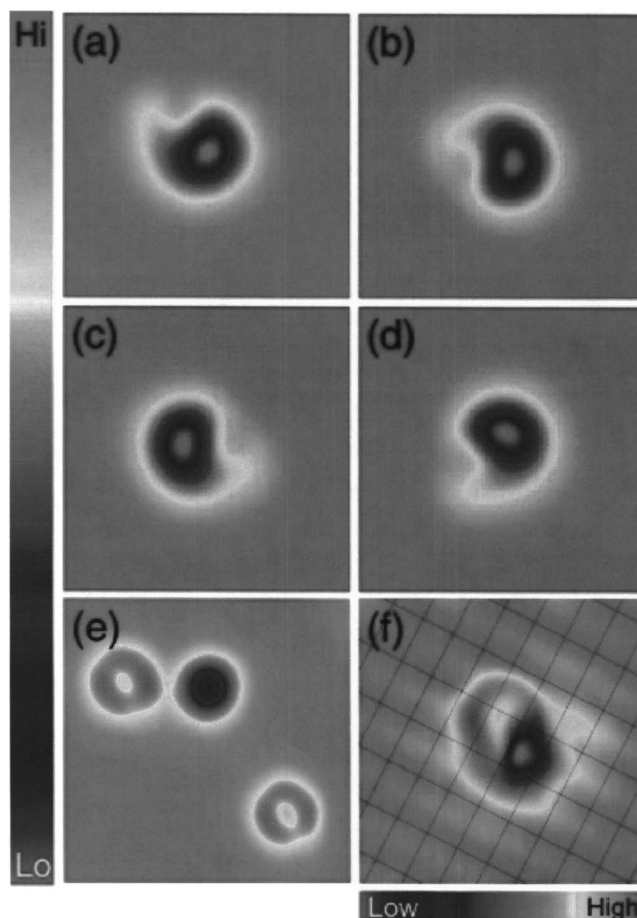


FIG. 5. [(a)–(d)] STM topographical images of four types of O₂–O_{sb} complexes. The images were obtained using a bare metallic tip at a sample bias of 70 mV and a tunneling current of 1 nA. The scan area of the images [(a)–(d)] is 25×25 Å². (e) A voltage pulse of +420 mV on the complex led to the formation of three O atoms. (f) STM image taken using a CO-terminated tip for the complex shown in (a).

IV. DISCUSSION

A. Adsorption of O₂ molecules

O₂ molecules physisorb onto a Ag(110) surface at temperatures below 40 K.^{6,7} In our experiments on physisorption of O₂ at 13 K,³⁰ we found that the weakly bonded physisorbed molecules diffused across the surface until they encountered an impurity, after which they were attached to the impurity to form an island. Such mobility and weak binding on the surface led to unstable STM images. For chemisorbed O₂ molecules, it is well established that the molecular axis is parallel to the surface; however, the details regarding the O₂ orientation and adsorption site have been a matter of debate.^{8–16} Recent density-functional theory (DFT) calculations^{12,13} revealed that the optimal adsorption site is the fourfold hollow site and that adsorption energies are 0.51 and 0.55 eV for the $[1\bar{1}0]$ and $[001]$ orientations, respectively. However, within the accuracy of the calculations the two orientations thus appear equally likely. Such a very slight difference in energy might cause some conflicts in the assignment of the orientations from experimental results. Outka *et al.*⁹ assumed the molecular axis to align only along the $[1\bar{1}0]$ direction whereas an electron stimulated desorp-

tion ion angular distribution study¹¹ provided evidence for the [001] alignment of the O₂ molecules. Gravil *et al.* suggested¹³ that the slight difference in the calculated adsorption energies could be reconciled with previous experiments, if one assumes that the relative populations of the two O₂ orientations depend on the procedure used to prepare the chemisorbed state. Recent combined HREELS/temperature programmed desorption experiments were interpreted along the same lines,¹⁶ where they concluded that two chemisorbed states can be produced by direct adsorption above 40 K. Figure 1 shows direct evidences of the existence of the two types of O₂ molecules (produced by direct adsorption at 45–70 K) and the adsorption sites and orientations of the O₂ molecules. Two vibrational modes were observed on O₂(001) molecules using STM inelastic electron tunneling spectroscopy,²⁹ whereas no vibrations were found on O₂(110).

One interesting correlation in the characteristics of the system of O₂ adsorbed on Ag(110) is that the ratio of the number of O₂(001) to the number of O₂(110) is 0.71, which is the same as the ratio of the lattice distances along the [001] and [110] directions (2.89 and 4.09 Å for [001] and [110], respectively). This suggests the possibility that the orientation of the O₂ on the Ag(110) surface is determined by the direction at which the O₂ molecule impinges on the surface during adsorption. Assuming that the orientations of the gas phase molecules are statistically distributed and that the energy barrier to rotation is at the diagonal of the unit cell,¹³ the wider lattice spacing along the [001] direction may lead to a greater population of O₂(110). This is possible because the barrier to rotation along the diagonal in the unit cell (~0.6 eV) (Refs. 12 and 13) is higher than the estimated adsorption energy (~0.4 eV).¹³

B. Dissociation pathways of O₂ molecules

In previous work¹⁷ on the thermal dissociation of O₂ on a Ag(110) surface, it has been assumed that the trajectories of the O atoms during dissociation follow the direction predetermined by the molecular axis. Such behavior is observed in the present work when a negative voltage pulse is applied to O₂(001). However, application of a positive voltage pulse to O₂(001) first causes the molecule to rotate to form O₂(110), which then undergoes dissociation. Hence dissociation occurs along a direction perpendicular to the original O₂(001) molecular axis. Such contrasting dissociation pathways involve the $1\pi_g^+$ antibonding orbital resonance, which is located at the Fermi level of the O₂(001) on Ag(110).³¹ This resonance is also involved in STM imaging³¹ and vibrations²⁹ of the O₂(001) such as the O–O stretch and the antisymmetric O₂–Ag stretch. Such orbital resonance will also favor dissociation of O₂(001). The threshold voltages that resulted in dissociation in the present work (–390 and 470 mV at 1 nA tunneling current) correspond to the energy of the highest projected density of states on the O₂(001) $1\pi_g^+$ orbital.³¹ Therefore, the contrasting dissociation behavior of O₂(001) depending on the polarity of voltage pulse is associated with the molecular orbital;³² it is the injection of elec-

trons into this orbital that causes the rotation. It should be noted that O₂(110) molecules always dissociate along the [110] direction regardless of the sign of the voltage pulse. The observation of such dissociation pathways confirms the assignment of the orientation of the two types of the O₂ molecule.

The average atomic separation after the dissociation induced by the negative voltage pulse was 10.7 Å (25 s period at a bias voltage pulse of –390 mV and tunneling current of 1 nA), which is about ~1.5 (2.2) times of a lattice space along the [110]([001]) direction. In contrast, the average atomic separation resulting from the positive voltage pulse was only 4.3 Å (25 s period at a bias voltage pulse of 470 mV and a tunneling current of 1 nA). This difference in atomic separations of positive/negative voltage pulses may present one of surface anisotropy effects on dissociation dynamics. The interpair separation after thermal dissociation of O₂ on Pt(111),³³ Cu(110),³⁴ Rh(001),³⁵ and Ag(110) (Ref. 17) is more than one lattice constant, and is similar to that of tunneling-electron-induced dissociation.^{36,37} The higher than expected atomic separation after thermal dissociation observed in the present work suggests the existence of hot atoms produced by the transfer of adsorption energy into kinetic energy. The larger separation observed along the [001] direction could be due to the higher mobility of O_{sb}.

C. Diffusion of oxygen atoms

The O_{sb} was not observed in the thermal dissociation results at 170 K that O₂ dissociated into two O_{fth} along the [001] direction.¹⁷ We found that O_{sb} undergoes thermal diffusive motion even at 13 K, moving up to two lattice spacings within an hour, whereas O_{fth} is very stable. Formation of O_{sb} may be associated with a higher corrugated surface potential along the [001] direction. Because of the higher potential corrugations, extension of the O–O bond for dissociation along the [001] direction makes it possible to produce the O_{fth}–O_{sb} complex. In the present experiments, O_{sb} was produced by thermal dissociation at 45–75 K (6% in Table I). The high mobility of O_{sb} may play an important role in added-row surface reconstruction at elevated temperatures.

We observed that O_{sb} atoms always diffused between short-bridge sites, regardless of whether they diffuse along the [001] or [110] direction. This indicates that the O_{sb} atoms have a higher barrier for diffusion to fourfold hollow sites than to other short-bridge sites. Therefore, when O_{sb} diffuses along the [001] direction it must bypass the fourfold hollow site.

O_{fth} atoms are highly reactive to adsorbed CO molecules³⁸ whereas O_{sb} are not. The CO molecule can be positioned with the STM at various distances from the O_{fth} and the O_{sb}. At the closest separation, CO₂ production can be induced by tunneling electrons with the O_{fth}.³⁸ However, no reaction was observed between the CO and the O_{sb} even though the O_{sb} diffuses to the CO very closely. The different reactivities of O_{fth} and O_{sb} with CO are consistent with the prediction by Burghaus and Conrad that two atomic oxygen species with slightly different reactivities exist on the Ag(110) surface.^{23,24} They made this prediction on the basis

of experiments in which, after dissociative O₂ adsorption at 180 K, a CO molecular beam was directed at the Ag(110) surface. They observed CO₂ production, but the reaction rate showed unexpectedly complex behavior as a function of exposure. These observations led them to conclude that two atomic oxygen species existed on the surface.

V. SUMMARY

In a STM study of the chemisorption and dissociation of single O₂ molecules on a Ag(110) surface, we directly observed two types of O₂ molecule [O₂(001) and O₂(110)], two types of oxygen atom (O_{ffh} and O_{sb}), and the O₂-O_{sb} complex. The rotation and dissociation pathways of O₂(001) depend on the direction of electron tunneling. Furthermore, the dynamical features of the O_{sb} atoms, the O_{ffh}-O_{sb} complex, and the O₂-O_{sb} complex were observed. Our results provide insights into the adsorption, dissociation, and reaction dynamics of oxygen molecules and atoms, and these insights should be explored in future theoretical calculations.

ACKNOWLEDGMENT

This manuscript is based upon work supported by the Chemical Science, Geo- and Bioscience Division, Office of Science, U.S. Department of Energy (Grant No. DE-FG03-01ER15157).

¹J. Haber, in *Handbook of Heterogeneous Catalysis*, edited by G. Ertl, H. Knozinger, and J. Weitkamp (VCH, Weinheim, 1997), p. 2253.

²R. A. van Santen and H. P. C. Kuipers, *Adv. Catal.* **35**, 265 (1987).

³M.-L. Bocquet, A. Michaelides, D. Loffreda, P. Sautet, A. Alavi, and D. A. King, *J. Am. Chem. Soc.* **125**, 5620 (2003).

⁴S. Linic and M. A. Barteau, *J. Am. Chem. Soc.* **124**, 310 (2002).

⁵S. Linic, H. Piao, K. Adib, and M. A. Barteau, *Angew. Chem., Int. Ed.* **43**, 2918 (2004).

⁶C. T. Campbell, *Surf. Sci.* **157**, 43 (1985).

⁷K. C. Prince, G. Paolucci, and A. M. Bradshaw, *Surf. Sci.* **175**, 101 (1986).

⁸R. J. Guest, B. Hernns, P. Bennich, O. Bjrneholm, A. Nilsson, R. E. Palmer, and N. Mårtensson, *Surf. Sci.* **278**, 239 (1992).

⁹D. A. Outka, J. Stohr, W. Stark, P. Stevens, J. Solomon, and R. J. Madix, *Phys. Rev. B* **35**, 4119 (1987).

¹⁰J. Pawela-Crew, R. J. Madix, and J. Stohr, *Surf. Sci.* **339**, 23 (1995).

¹¹K. Bange, T. E. Madey, and J. K. Sass, *Chem. Phys. Lett.* **113**, 56 (1985).

¹²P. A. Gravil, J. A. White, and D. M. Bird, *Surf. Sci.* **352-354**, 248 (1996).

¹³P. A. Gravil, D. M. Bird, and J. A. White, *Phys. Rev. Lett.* **77**, 3933 (1996).

¹⁴P. J. van den Hoek and E. J. Baerends, *Surf. Sci.* **221**, L791 (1989).

¹⁵H. Nakatsuji and H. Nakai, *J. Chem. Phys.* **98**, 2423 (1991).

¹⁶F. Bartolucci, R. Franchy, J. C. Barnard, and R. E. Palmer, *Phys. Rev. Lett.* **80**, 5224 (1998).

¹⁷T. Zambelli, J. V. Barth, and J. Wintterlin, *J. Phys.: Condens. Matter* **14**, 4241 (2002).

¹⁸L. Vattuone, M. Rocca, and U. Valbusa, *Surf. Sci.* **314**, L904 (1994).

¹⁹M. Taniguchi, K. Tanaka, T. Hashizume, and T. Sakurai, *Surf. Sci.* **262**, L123 (1992).

²⁰T. Zambelli, J. V. Barth, and J. Wintterlin, *Phys. Rev. B* **58**, 12663 (1998).

²¹L. Vattuone, M. Rocca, P. Resteli, M. Pupo, C. Boragno, and U. Valbusa, *Phys. Rev. B* **49**, 5113 (1994); L. Vattuone, M. Rocca, C. Boragno, and U. Valbusa, *J. Chem. Phys.* **101**, 713 (1994).

²²L. Vattuone and M. Rocca, *Phys. Rev. B* **49**, 14744 (1994).

²³U. Burghaus and H. Conrad, *Surf. Sci.* **338**, L869 (1995).

²⁴U. Burghaus and H. Conrad, *Surf. Sci.* **370**, 17 (1997).

²⁵U. Burghaus and H. Conrad, *Surf. Sci.* **352**, 201 (1996).

²⁶The STM is a variation of the one described in B. C. Stipe, M. A. Rezaei, and W. Ho, *Rev. Sci. Instrum.* **70**, 137 (1999); L. J. Lauhon and W. Ho, *ibid.* **72**, 216 (2001).

²⁷H. J. Lee and W. Ho, *Science* **286**, 1719 (1999).

²⁸J. R. Hahn and W. Ho, *Phys. Rev. Lett.* **87**, 196102 (2001).

²⁹J. R. Hahn, H. J. Lee, and W. Ho, *Phys. Rev. Lett.* **85**, 1914 (2000).

³⁰J. R. Hahn and W. Ho (unpublished).

³¹F. E. Olsson, N. Lorente, and M. Persson, *Surf. Sci.* **522**, L27 (2002).

³²J. R. Hahn and W. Ho, *J. Chem. Phys.* **122**, 244704 (2005).

³³J. Wintterlin, R. Schuster, and G. Ertl, *Phys. Rev. Lett.* **77**, 123 (1996).

³⁴B. G. Brinner, M. Doering, H.-P. Rust, and A. M. Bradshaw, *Phys. Rev. Lett.* **78**, 1516 (1997).

³⁵S. W. Hla, P. Lacovig, G. Comelli, A. Baraldi, M. Kiskinova, and R. Rosei, *Phys. Rev. B* **60**, 7800 (1999).

³⁶B. C. Stipe, M. A. Rezaei, W. Ho, S. Gao, M. Persson, and B. I. Lundqvist, *Phys. Rev. Lett.* **78**, 4410 (1997).

³⁷B. C. Stipe, M. A. Rezaei, and W. Ho, *J. Chem. Phys.* **107**, 6443 (1997).

³⁸J. R. Hahn and W. Ho, *Phys. Rev. Lett.* **87**, 166102 (2001).